Presheath/sheath model with secondary electron emission from two parallel walls

E. Ahedo
E.T.S.I. Aeronáuticos, Universidad Politécnica de Madrid, 28040 Madrid, Spain

(Received 26 April 2002; accepted 5 July 2002)

A macroscopic model of the interaction of a plasma with two parallel, electron-emitting walls is presented. Zero Debye-length and total thermalization of the secondary electron emission (SEE) are assumed. The SEE is treated as a free beam within each thin, collisionless sheath, but as part of a single electron population within the presheath. Plasma models with three and two species result in sheath and presheath, respectively. The ion flow at the presheath/sheath transition is sonic, and the sound speed there determines the relation between the temperature of the confined electron populations in sheath and presheath. For the general case of a plasma flowing axially between two annular walls the complete dimensionless solution depends on five parameters. Potential drops in the presheath can be larger than in the sheaths, mainly when charge-saturation is reached in the sheath or for a large effective ion friction in the presheath. The losses of plasma current to the walls are determined totally by the presheath problem, whereas the sheath problem and wall material determine the energy lost by impacting particle. Energy losses change drastically from zero SEE to a SEE yield about 100% when the charge-saturated regime is reached. © *2002 American Institute of Physics.* [DOI: 10.1063/1.1503798]

I. INTRODUCTION

The transverse (or radial) interaction of a collisionless plasma with two dielectric walls confining it was treated originally by Tonks and Langmuir.[1] They developed the sheath/presheath asymptotic theory for the zero-Debye length limit and solved the fundamental issues of the problem. In the Tonks–Langmuir model, and later papers complementing it,[2–5] the ion and electron losses to the walls are balanced by volume ionization. Recently we generalized that model to plasmas flowing parallel to planar or annular walls.[6] The presheath solution depends then on two new parameters related to the axial flow, and it is shown that (i) in the absence (or excess) of ionization, the axial flow balances the radial losses of particles to the walls, and (ii) axial gradients introduce a friction effect on the radial acceleration of the ions, which leads to larger potential drops in the presheath and lower losses to the walls.

The above models consider implicitly that the plasma is confined between two passive (i.e., nonemitting) walls. However, in many cases electron emission by the wall is important. For certain materials, electron impact produces a secondary electron emission (SEE) yield (i.e., the ratio between the secondary and primary electron fluxes at the wall) above 100%.[7,8] Secondary electrons interact with the electrostatic field and the main plasma, and modify sheath and presheath characteristics.

The collisionless sheath with SEE was studied originally by Hobbs and Wesson,[9] who demonstrated that the sheath becomes charge-saturated for a SEE yield close to 100%. However, they treated the sheath exclusively and did not propose any model of the presheath with SEE. To close the sheath problem at the sheath/plasma boundary, they imposed the usual quasineutrality condition and a generalized form of the Bohm condition.

Schwager formulated a planar, kinetic model with secondary emission of the region between one emitting wall and a source- or edge-plasma.[10] That region consisted of a (negative) wall sheath, followed by a quasineutral region, and a (positive) sheath next to the edge-plasma. Stephens and Ordonez studied practically the same model,[11] and Jolivet and Roussel applied the last one to the case of a Hall thruster.[7] In these three models, secondary electrons are assumed to accelerate freely across the whole plasma region between the emission wall and the edge-plasma. The secondary population is thermalized at the edge-plasma and re-emitted back as primary electrons to the central plasma region. This wall plus edge-plasma model does not apply satisfactorily to the case of a plasma confined between two walls, with no intermediate edge-plasma. First, in a planar geometry this edge-plasma should act as a symmetry surface, which it certainly does not; the secondary population behaves like a "free" beam in its way to the channel center, but as part of the main, "thermalized" electron population in the way back from the center. Second, the edge-plasma tends to create a sheath-like region close to it, which is not expected in the (typical) two-wall case.

As the works just commented suggest, the main difficulty lies in the treatment of the SEE in the bulk of the plasma. Recently, we suggested that the presheath/sheath theory is very suitable to formulate a consistent model with SEE, since the existence of two very different regions allows one to model differently the secondary electron population in each region.[12] The present paper develops in detail the model for the case of total thermalization of the SEE.

An envisaged application of the resulting model is the

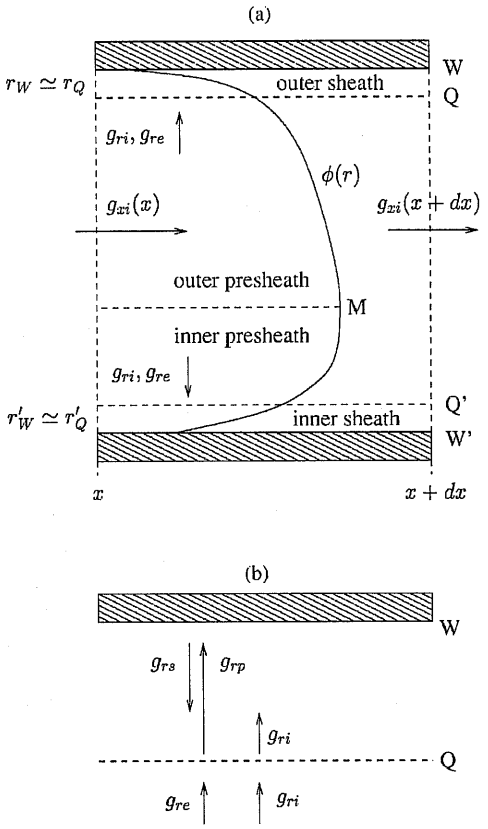

FIG. 1. (a) A generic radial section of a long annular channel between two dielectric walls; g_x and g_r represent axial and radial particle fluxes, respectively; $\phi(r)$ sketches the electric potential, which is maximum at an intermediate point M; points Q and Q' represent the transitions to the two sheaths. (b) Treatment of the electrons in presheath and sheaths: in each sheath, primary (p) and secondary (s) populations are defined; in the presheath, a single population (e) is defined; zero-current plus flux conservation conditions at each presheath/sheath transition yield $g_{riQ}=g_{reQ}=g_{rpQ}+g_{rsQ}$, and similarly for point Q'.

plasma discharge in a Hall thruster chamber made of ceramic walls. The discharge is axisymmetric and particle and energy losses to the walls are known to effect greatly the thruster performance.[13–16] Therefore, a good understanding of the radial plasma–wall interaction is crucial to predict correctly the axial response of the discharge.

The rest of the paper is organized as follows: In Sec. II we formulate the main hypotheses of the model. In Sec. III we discuss the sheath solution. In Sec. IV we match the presheath model to the sheath solution and we compute results for the complete solution. In Sec. V we discuss the main results.

II. MODEL FORMULATION

Figure 1(a) sketches the radial model. The plasma flows between two annular walls placed, in cylindrical coordinates (x,r,θ), at $r=r_{W'}$ and $r=r_W=r_{W'}+h_c$, with h_c the channel width. Here we are interested in the radial structure of the plasma discharge at a given axial position x. For dielectric walls, the zero current condition implies, in general, the potential profile $\phi(r)$ to present a maximum at a central point of the channel [point M in Fig. 1(a)] and to decrease monotonically towards the two walls [points W and W']. Except for very large voltages, SEE is due mainly to the impact of those electrons from the main population with enough energy to reach the walls.

For a monotonic potential profile, secondary electrons are accelerated away from the walls by the radial electric field. Their later evolution inside the channel depends on the interaction with the rest of the plasma and with the electric field. Here we consider the case of both zero Debye-length and total thermalization (or total trapping) characterized by

$$\lambda_d \ll \lambda_{\mathrm{col}} \ll h_c , \tag{1}$$

where λ_d is the Debye length and λ_{col} is the effective mean free-path for the SEE. Collisions of secondary electrons with ions or neutrals transform the radial kinetic energy gained from the electric field into random (i.e., thermal) energy. This decrease in radial energy prevents one part of the SEE from reaching the opposite wall, remaining then trapped in the bulk of the plasma and thermalizing eventually with the main electron population. For the case $\lambda_{\mathrm{col}} \ll h_c$, we may consider that the whole secondary population thermalizes.

The first inequality in Eq. (1) allows us to apply the presheath/sheath theory to the problem. That theory presents three features that are very adequate for a dual modeling of the trapped SEE: (i) presheath and sheath problems are formulated and solved independently in their own scales, (ii) the sheaths are surface discontinuities (tied to the walls) in the quasineutral scale, but collisionless layers in their inner scale; and (iii) the matching or transition condition between presheath and sheath is unique and consists of a sonic (or Bohm) condition on the ion flow (for a plasma with zero radial flow somewhere in the presheath).[6,9,17]

For the total thermalization case, we propose to model the electron populations in the following way:

(i) There are two independent populations of electrons within each thin, collisionless sheath: population p of primary, confined electrons, coming from the bulk of the plasma, and population s of secondary, wall-emitted electrons. Population p is assumed in Maxwell–Boltzmann equilibrium at temperature T_p, whereas population s is accelerated freely by the sheath potential from the wall to the presheath boundary.

(ii) The whole SEE remains trapped within the plasma. The final, steady state of this trapped population is to thermalize with the main electron population. Therefore, within the presheath, we group all (trapped) electrons, irrespective of their origin (ionization, axial flow, or wall-emission), in a single population e, which is in Maxwell–Boltzmann equilibrium at temperature T_e.

(iii) To match consistently the solutions of presheath and sheaths three basic laws are imposed at each presheath/sheath transition: the conservation of the total electron density, the conservation of the net electron flux, and the sonic transition of the ion flux.

In this formulation, the populations p and e of confined electrons in sheath and presheath are not identical (except for zero SEE), having different densities at the transition surface and different temperatures. Furthermore, for an asymmetric presheath, populations p and s in each sheath do not coincide too. The relation between T_p for each p-population and T_e must be determined as part of the solution. The same ion population (i) is considered in sheath and presheath, and this is accelerated by the electric field from around the center of the channel towards the two walls. Thus, a three-species plasma is used in each sheath, and a two-species one in the presheath. The Hobbs–Wesson model can be applied to each sheath, whereas usual models for two-species plasmas can be considered for the presheath. Here, we will use the general presheath model of Ref. 6, which admits axial plasma flows and asymmetric solutions.

III. SHEATH ANALYSIS

A. Sheath solution

In general, we will refer the discussion to the sheath tied to the outer wall; the inner sheath behaves in the same way. The outer sheath extends from the the wall (point W) to the presheath transition (point Q). If the sheath is not charge-saturated the electric potential is monotonic with $\phi_{WQ}=\phi_Q-\phi_W>0$. In the zero Debye-length limit of Eq. (1), the sheath satisfies the conservation equations,

$$n_i v_{ri}=\text{const}=g_{riQ}, \tag{2}$$

$$m_i v_{ri}^2/2+5T_i/2+e\phi=\text{const}, \tag{3}$$

$$n_i^{-2/3}T_i=\text{const}, \tag{4}$$

$$n_p=n_{pW}\exp\frac{e\phi-e\phi_W}{T_p}, \tag{5}$$

$$n_s v_{rs}=\text{const}=g_{rsW}, \tag{6}$$

$$m_e v_{rs}^2/2-e\phi=\text{const}, \tag{7}$$

the flux conditions,

$$g_{riQ}=g_{rpW}+g_{rsW}, \tag{8}$$

$$g_{rpW}=(T_p/2\pi m_e)^{1/2}n_{pW}, \tag{9}$$

$$g_{rsW}=-\delta_w(T_p)g_{rpW}, \tag{10}$$

and the (quasiplanar) Poisson equation,

$$\frac{d^2\phi}{dr^2}=\frac{e}{\epsilon_0}(n_p+n_s-n_i). \tag{11}$$

The constants for the ion equations (2)–(4) are set at point Q and match the values obtained at the presheath side. Since the wall temperature, T_w, is generally much smaller than the electron temperature, T_p, the mean energy of the secondary electrons when they leave the wall can be neglected in Eq. (7)—except in the very vicinity of point W. Equation (8) is the zero-current condition, and Eq. (9) corresponds to take a quasi-Maxwellian distribution for population p.

In Eq. (10), the effective SEE yield of the wall, $\delta_w(T_p)$, depends on both T_p and the wall material. For the present purposes and moderate electron energies, a good-enough expression of the emission yield produced by a monoenergetic beam of energy E per electron is $\delta_w(E)\simeq\sqrt{E/E_1}$, with E_1 the temperature for 100% yield (in the range $E_1\sim 10-100$ V, say).[7,14] Averaging over the quasi-Maxwellian population p the effective yield satisfies

$$\delta_w(T_p)\simeq\sqrt{T_p/T_1}, \tag{12}$$

with $T_1\sim 0.57E_1$. This last relationship allows us to use T_1/T_p instead of δ_w as input parameter for the sheath problem.

From Poisson equation (11), the convenient spatial variable in the sheath is

$$\zeta=\frac{r-r_W}{\lambda_d}, \tag{13}$$

with $\lambda_d=\sqrt{\epsilon_0 T_p/e^2 n_{iQ}}$. The integration of Eq. (11) together with Eqs. (2)–(7) yields the conservation equation

$$\frac{e^2 n_{iQ}}{2T_p}\left[\left(\frac{d\phi}{d\zeta}\right)^2-\left(\frac{d\phi}{d\zeta}\right)_Q^2\right]=U(e\phi)-U(e\phi_Q), \tag{14}$$

with

$$U(e\phi)=n_pT_p+n_sm_ev_{rs}^2+n_i(m_iv_{ri}^2+T_i) \tag{15}$$

the Sagdeev's potential.[18] First and second derivatives of this function are

$$\begin{aligned} U'(e\phi)&=n_p+n_s-n_i,\\ U''(e\phi)&=\frac{n_p}{T_p}-\frac{n_s}{m_ev_{rs}^2}-\frac{n_i}{m_iv_{ri}^2-\frac{5}{3}T_i}. \end{aligned} \tag{16}$$

There are three boundary conditions related to Eq. (14). First, plasma quasineutrality at point Q yields

$$U_Q'=0. \tag{17}$$

Second, for a solution to exist around point Q with $|d\phi/d\zeta|$ increasing towards the wall, Eq. (14) requires that $U_Q''\geqslant 0$. In terms of the ion velocity (and neglecting the case $m_iv_{riQ}^2<\frac{5}{3}T_{iQ}$ which does not lead to a valid solution at the wall) this condition is equivalent to

$$m_iv_{riQ}^2\geqslant\frac{5}{3}T_{iQ}+T_p\frac{n_{pQ}+n_{sQ}}{n_{pQ}-n_{sQ}T_p/(2e\phi_{WQ})}, \tag{18}$$

which is the Bohm sonic/supersonic condition for the present three-species plasma. Since the quasineutral solution of the presheath accepts only a subsonic/sonic transition (see Sec. IV B), the sonic condition,

$$U_Q''=0, \tag{19}$$

is the correct one for the sheath/presheath transition. Finally, the analysis of the transition region around point Q shows that the electric field, when measured in the sheath scale, tends asymptotically to zero at the sheath boundary[17,19]

$$\left.\frac{d(e\phi/T_p)}{d\zeta}\right|_Q\sim\frac{\lambda_d}{d}\to 0. \tag{20}$$

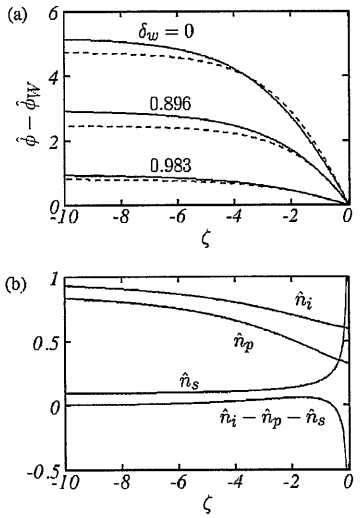

FIG. 2. (a) Potential profile for different values of the secondary emission yield and $\hat{T}_{iQ}=0$ (solid lines) and 1 (dashed lines). The cases $\delta_w = \delta_w^*(\hat{T}_{iQ})$ correspond to $d\hat{\phi}/d\zeta|_W=0$, marking the charge-saturation limit of the sheath. (b) Profiles of the different plasma species for $\hat{T}_{iQ}=0$ and $\delta_w=\delta_w^*$; $\hat{n}_i-\hat{n}_p-\hat{n}_s$ is the local electric charge in the sheath.

From the preceding equations and conditions, the dimensionless solution of the sheath depends on just two parameters, δ_w (or T_1/T_p) and $\hat{T}_{iQ}\equiv T_{iQ}/T_p$. Hobbs and Wesson treated the case of cold ions, $\hat{T}_{iQ}=0$. Figure 2(a) shows potential profiles for different emission yields and two ion temperatures. For a given potential and according to Eq. (3), a warm ion population has a larger density and a lower velocity than a cold one; this implies a smaller Debye length (i.e., a shorter sheath) and a lower potential drop. Figure 2(b) shows, for a particular case, the profiles of the different densities and of the net electric charge; notice the change of sign of the local electric charge and the sharp decrease of n_s as the presheath is approached.

Figures 3(a)–3(c) show, for two ion temperatures, the evolution of three relevant sheath parameters with the secondary emission yield. For $\delta_w<0.9$, roughly, the sheath potential drop and the electric field at the wall decrease slowly with δ_w, and the fractional density of secondary electrons delivered to the presheath is negligible; notice that the electric field at the wall increases with $\hat{T}_{iQ}$ in spite of the lower potential drop. The behavior of ϕ_{WQ} with δ_w is easy to explain from the expression,

$$\hat{\phi}_{WQ}\equiv\frac{e\phi_{WQ}}{T_p}=\ln\sqrt{\frac{m_i}{2\pi m_e}}+\ln(1-\delta_w)+\ln\left(\frac{n_{pQ}\sqrt{T_p/m_i}}{n_{iQ}\ v_{riQ}}\right), \tag{21}$$

derived from Eqs. (8)–(10). Because of the large ion-to-electron mass, ϕ_{WQ} and $d\phi/d\zeta|_W$ do not change drastically with δ_w until $1-\delta_w$ becomes of the order of $\sqrt{m_e/m_i}$.

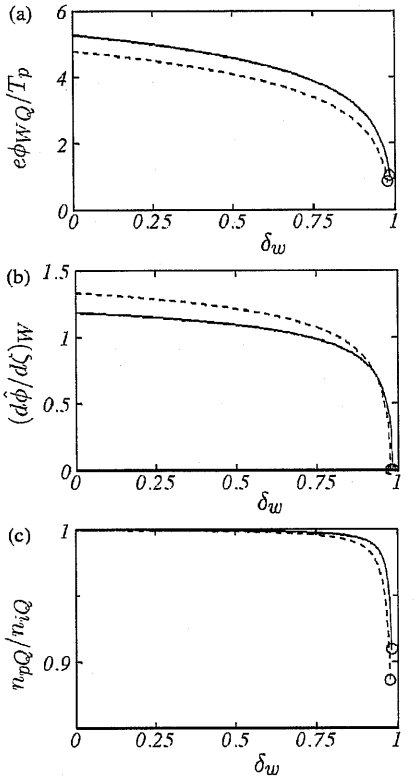

FIG. 3. Evolution with δ_w of the sheath potential drop, the electric field at the wall, and the density of secondary electrons at point Q for $\hat{T}_{iQ}=0$ (solid lines) and 1 (dashed lines). Circles correspond to the charge saturation limit. At this limit $\hat{\phi}^*_{WQ}$ goes from 1.02 at $\hat{T}_{iQ}=0$ to 0.846 at $\hat{T}_{iQ}=1$.

B. The charge-saturated regime (CSR)

The sheath reaches the charge saturation limit (CSL) when the electric field at the wall becomes zero. For $\hat{T}_{iQ}=0$, Hobbs and Wesson found that the CSL is reached when the SEE yield and the potential drop are

$$\delta_w=\delta_w^*\simeq 1-8.3\sqrt{\frac{m_e}{m_i}},\quad \frac{e\phi_{WQ}}{T_p}=\hat{\phi}^*_{WQ}\simeq 1.02. \tag{22}$$

For warm ions, we find that $\hat{T}_{iQ}$ has an irrelevant influence on the value of δ_w at the CSL; for xenon, one has $\delta_w^*\simeq 0.983$ for $\hat{T}_{iQ}=0$ and $\delta_w^*\simeq 0.981$ for $\hat{T}_{iQ}=1$. The effect of $\hat{T}_{iQ}$ on other magnitudes is small but not negligible; the sheath potential drop at the CSL, $\hat{\phi}^*_{WQ}(\hat{T}_{iQ})$, decreases about 17% when $\hat{T}_{iQ}$ goes from 0 to 1.

For $\delta_w>\delta_w^*$ the sheath is in the charge-saturated regime (CSR). A potential well is formed near the wall to turn back the excess of secondary flux. Its magnitude, $\Delta\phi_W$, must be such that, at the point of minimum potential, the secondary flux takes the CSL value, $-\delta_w^* g_{rp|W}$. A simple estimate yields

$$\Delta\phi_W\sim(T_w/e)\ln(\delta_w/\delta_w^*). \tag{23}$$

Then, in the asymptotic limit $T_w/T_p \to 0$, the potential well can be neglected and the dimensionless solution for the whole charge-saturated regime (CSR) coincides with that of the CSL. In particular, one has

$$\frac{e\phi_{WQ}}{T_p} = \text{const} = \hat{\phi}^*_{WQ}(\hat{T}_{iQ}), \quad g_{rsQ} = -\delta^*_w g_{rpW}, \tag{24}$$

for the whole CSR.

Let us come back to the the physical interpretation of the CSL. This limit corresponds to the total electric charge inside the sheath being zero, the sheath becoming thus a double-layer.[18] An additional interpretation of the CSL is obtained from Eq. (14), which states the conservation of the radial momentum of the whole plasma across the sheath. Then, the CSL corresponds to equal plasma momentum at both sheath ends,

$$0 = U(e\phi_W) - U(e\phi_Q). \tag{25}$$

From the definition of $U(e\phi)$, we may write

$$U(e\phi_W) - U(e\phi_Q) \equiv \Delta P_i + \Delta P_p + \Delta P_s, \tag{26}$$

with

$$\begin{aligned} \Delta P_i &= g_{riQ}\sqrt{2e\phi_{WQ}m_i} \times \sqrt{1+\frac{m_i v_{iQ}^2}{2e\phi_{WQ}}}\left(1-\frac{v_{iQ}}{v_{iW}}\right), \\ \Delta P_p &= g_{riQ}\sqrt{T_p m_i} \times \frac{n_{pQ}}{n_{iQ}} \sqrt{\frac{T_p}{m_i v_{iQ}^2}}\left(1-\frac{n_{pW}}{n_{pQ}}\right), \\ \Delta P_s &= |g_{rsW}|\sqrt{2e\phi_{WQ}m_e}, \end{aligned} \tag{27}$$

the jumps of dynamic pressure for the different species between the two sheath boundaries. For $\delta_w < 1$, one has $e\phi_{WQ} \gg T_p$, ΔP_i dominates clearly in Eq. (26), and charge-saturation cannot be reached. Population p, by itself, never compensates the ion term, ΔP_i. As for the effect of the SEE, one has $\Delta P_s \sim \Delta P_i$ when

$$|g_{riQ}|/|g_{rsW}| \sim \sqrt{m_e/m_i}, \tag{28}$$

in agreement, within order-of-magnitude, with the exact condition for the CSL: $g_{riQ}/|g_{rsW}| \simeq 8.3\sqrt{m_e/m_i}$. Thus, up to dominant terms, Eq. (25) states that the ion momentum at the wall is balanced by the momentum of population s and the pressure of population p at the presheath boundary. Notice that Eq. (28) coincides with the well-known Langmuir condition for a strong, stationary double-layer (characterized by $e\phi_{WQ}/T_p \gg 1$).[17]

Finally, we point out that the sheath solution is universal for any g_{riQ}, that is for any plasma current entering the sheath. This means that g_{riQ} is determined by the presheath solution and is unaffected by δ_w. On the contrary, as δ_w increases, both g_{rpW} and g_{rsW} change drastically, going from $|g_{rsW}| \ll g_{rpW} \simeq g_{riQ}$ at $\delta_w \ll 1$ to $|g_{rsW}| \simeq g_{rpW} \gg g_{riQ}$ at $\delta_w \simeq \delta^*_w$.

IV. COMPLETE SOLUTION

A. Presheath solution

For total thermalization of the SEE, the quasineutral plasma of the presheath consists of (i) the population i of ions, which are accelerated from point M of maximum potential and zero ion velocity towards the sheath transition points Q' and Q, and (ii) a single population e of confined electrons, which are in Maxwell–Boltzmann equilibrium at temperature T_e. According to Ref. 6, for the general case of a plasma flowing axially between two annular walls, the presheath problem depends on the channel geometry (annular ratio $\beta = r_{W'}/r_W$, and channel width h_c), the plasma conditions (ion density and temperature at point M, n_{iM} and T_{iM}, and electron temperature T_e), and the effective frequencies for net plasma production (ν_w), ionization (ν_i), and radial friction (ν_r). The presheath problem states that the transition to the (outer) sheath is defined by the sonic Bohm condition[6,17]

$$m_i v_{riQ}^2 = 5T_{iQ}/3 + T_e. \tag{29}$$

Using dimensionless variables, the presheath solution depends on just four parameters: β, $\tilde{T}_{iM} \equiv T_{iM}/T_e$, $\tilde{\nu}_i \equiv \nu_i/\nu_0$, and $\tilde{\nu}_r \equiv \nu_r/\nu_0$, with $\nu_0 = h_c^{-1}\sqrt{T_e/m_i}$. In particular, the relationship

$$\tilde{\nu}_w = \tilde{\nu}_w(\beta, \tilde{T}_{iM}, \tilde{\nu}_i, \tilde{\nu}_r) \tag{30}$$

is known as the plasma balance equation. For the no-flowing case of Tonks–Langmuir, one has $\tilde{\nu}_w = \tilde{\nu}_i = \tilde{\nu}_r$ and the plasma balance equation reduces to $\tilde{\nu}_i(\beta, \tilde{T}_{iM})$. Figure 5, commented below, illustrates the presheath solution with a particular example.

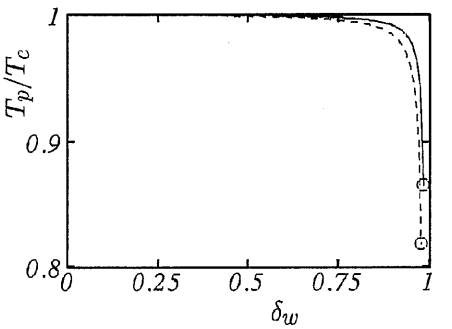

FIG. 4. Evolution with δ_w of the temperature ratio for the confined electron populations p (of the sheath) and e (of the presheath) for $\hat{T}_{iQ}=0$ (solid lines) and 1 (dashed lines). At the CSL, T_p/T_e goes from 0.865 at $\hat{T}_{iQ}=0$ to 0.819 at $\hat{T}_{iQ}=1$.

B. Presheath/sheath matching

The correct matching of the presheath and sheath solutions comes out from three basic conservation equations, which, in fact, have been imposed already. First, the conservation of electron particles and fluxes yields

$$n_{pQ} + n_{sQ} = n_{eQ} = n_{iQ}, \quad g_{rpQ} + g_{rsQ} = g_{reQ}.$$

Then, the fulfillment of the sonic Bohm conditions at the sheath and presheath sides, Eqs. (19) and (29), yields

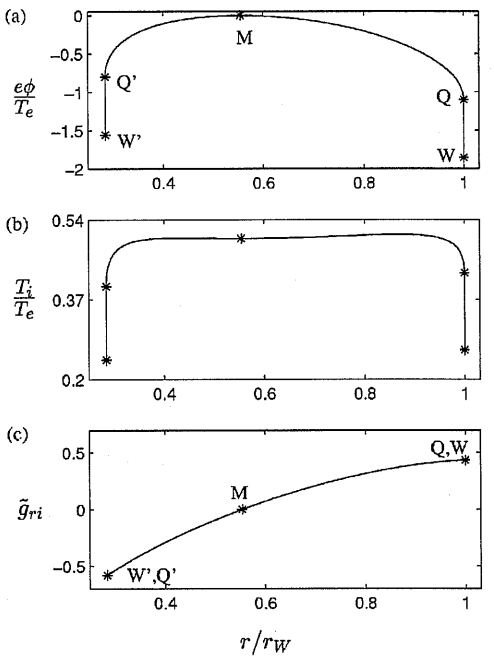

FIG. 5. Complete presheath/sheaths solution in the quasineutral scale for an annular channel with $\beta=0.285$, $T_{iM}/T_e=0.50$, $\tilde{\nu}_r=\tilde{\nu}_i=3.49$, and charge-saturated conditions at the two sheaths, $Q'W'$ and QW. In (c) $\tilde{g}_{ri}=(n_{iM}\sqrt{T_e/m_i})^{-1}g_{ri}$ is the dimensionless flux, which is constant across each sheath.

$$\frac{n_{eQ}}{T_e}=\frac{n_{pQ}}{T_p}-\frac{n_{sQ}}{2e\phi_{WQ}} \tag{31}$$

or, solving for $T_p(T_e)$,

$$\frac{T_p}{T_e}=1-\frac{n_{sQ}}{n_{iQ}}\left(1+\frac{T_p}{2e\phi_{WQ}}\right)<1. \tag{32}$$

Figure 4 illustrates the evolution of T_p/T_e with δ_w and $\hat{T}_{iQ}$, which is very similar to that of n_{pQ}/n_{iQ} shown in Fig. 3(c).

The fulfillment of sonic conditions at the presheath/sheath transition is essential for the continuity of the ion flow, as we justify next. For $\delta_w=0$, populations p and e coincide, as expected, and Eqs. (19) and (29) are exactly the same condition. It is then well established that the ion flow can be neither supersonic inside the presheath, nor subsonic inside the sheath, so that a sonic ion flow is the only possible transition.[1,6,19] The sound speed for a two-species plasmas, Eq. (29), is made up of the contributions of the ion pressure and the electron pressure (this last one through the electrostatic interaction between ions and electrons). For $\delta_w>0$, there are three plasma species in the sheath and the electrostatic interaction of the ions with the two electron populations becomes more complex. This is reflected by the expression of the sound speed in Eq. (18), which includes contributions of the ion pressure, the pressure of population p, and the dynamic pressure of the SEE. It can be shown that when a three-species plasma is considered in both presheath and sheath, the sonic condition, with a generalized sound speed of the form of the one used in Eq. (18), continues to yield the only correct transition. The peculiarity of the present model lies in the plasma being treated as a two-species one in the presheath and as a three-species one in the sheath. Our postulate is that the sonic condition, being a fundamental one for the plasma flow, must be satisfied in this case too. The consequence is that for the two different expressions of the sound speed to coincide at point Q, the temperatures of populations p and e must follow Eq. (32). This condition is not a parameter restriction but the relationship needed to close the model.

The way we have followed to relate the two electron temperatures (and pressures) is the natural one to our macroscopic approach, more appropriate than a method based on the distribution functions of electrons at the two sides of point Q. In addition, our procedure complies with two reasonable energy considerations: (i) T_e is computed from the weighted harmonic mean of the radial energies of electrons of type p and s, Eq. (31), and (ii) confined population e, which receives the radial energy of population s, is hotter than population p, Eq. (32). Finally, the fact that both n_{pQ}/n_{eQ} and T_p/T_e are close to one, even at the CSR, leads us to conclude that the details of the macroscopic modeling of the SEE are not critical for the overall model.

In a recent two-dimensional model of the plasma discharge in a Hall thruster, Keidar *et al.* use a radial presheath/sheath model with secondary emission.[20] Their formulation is similar to ours for cold-ions ($T_i=0$) but the presheath/sheath matching is solved unsatisfactorily. First, they do not explain how they relate the trapped populations in sheaths and presheath and just take $T_p=T_e$, even at the CSR. Second and more important, they impose a subsonic ion flow at the sheath entrance, violating the supersonic/sonic condition (18). The authors do not show radial profiles to support their hypotheses.

C. Results and energy balance

Figure 5 shows an example of a matched sheath/presheath solution for an annular channel. Profiles are shown in the presheath scale, where the sheaths are two wall discontinuities; it is worth noting that the sheaths are semi-infinite in the inner scale ($\zeta_Q=-\infty$ in Fig. 2). Wall conditions (i.e., T_1) in Fig. 5 have been chosen such that the two sheaths are in the CSR. The profiles of the inner and outer presheaths are asymmetrical: larger potential drops and lower currents are found in the outer presheath. The presheath asymmetry introduces a very small asymmetry between the two sheaths: one has $T_p/T_e\simeq 0.837$ and $e\phi_{W'Q'}/T_e\simeq 0.759$ in the inner sheath, and $T_p/T_e\simeq 0.836$ and $e\phi_{WQ}/T_e\simeq 0.753$ in the outer one. An important feature is that the potential drop in the presheath is not negligible at all; indeed, in Fig. 5, the potential drop in the outer presheath is larger than in the sheaths, $\phi_{QM}>\phi_{W'Q'}$. The profile of the ion temperature illustrates the competition between the heating effect due to ionization and the cooling effect due to rarefaction, this last one dominating totally in the sheaths and justifying the small effect of the ion temperature on the sheath profiles.

The sheath solution showed that the relative potential drop $e\phi_{WQ}/T_p$ decreases as δ_w increases and remains con-

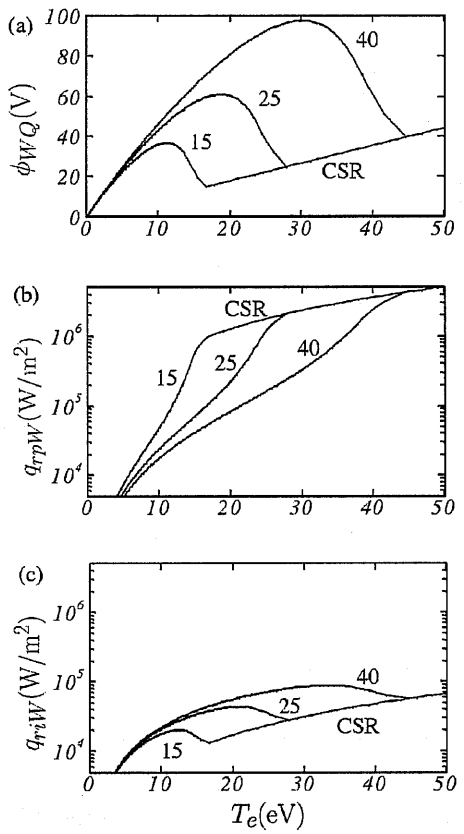

FIG. 6. (a) Sheath potential drop, (b) electron energy losses, and (c) ion energy losses as function of T_e for xenon, $T_{iQ}/T_e=0$, and three wall materials: $T_1=$ 15, 25 and 40 eV. The curves are independent of T_1 at the CSR. Plots (b) and (c) are for $n_{iQ}=10^{18}$ m^{-3}; for other densities, particle and energy losses scale proportional to n_{iQ}.

stant in the CSR. Figure 6(a) shows, for different wall materials, the evolution of the sheath potential drop with the electron temperature in the presheath, T_e. There is a relative maximum of $\phi_{WQ}(T_e)$, followed by a minimum just at the CSL, and then a linear increase with T_e: one has $e\phi^*_{WQ}/T_e \simeq 0.88$ (for xenon and $\hat{T}_{iQ}=0$). An important point is that ϕ_{WQ} is independent of the wall material once in the CSR. The potential drops in the presheaths, ϕ_{QM} and $\phi_{Q'M}$, must be computed from the presheath solution of Ref. 6.

Calling $q_{r\alpha W}$ the radial flux of energy of species α ($\alpha=i,p,s,e$) per unit of time, the energy fluxes of ions and electrons into the outer wall are

$$\begin{aligned} q_{riW}&=g_{riW}(\tfrac{1}{2}m_i v_{riW}^2+\tfrac{5}{2}T_{iW})\\ &=g_{riQ}(e\phi_{WQ}+\tfrac{1}{2}T_e+\tfrac{10}{3}T_{iQ}),\\ q_{rpW}&=g_{rpW}2T_p=g_{riQ}\frac{2T_p}{1-\delta_w}. \end{aligned} \tag{33}$$

Ion energy losses depend very weakly on the SEE yield since g_{riQ} is determined by the presheath. On the contrary, electron losses depend strongly on δ_w and do not dominate for a low SEE. Ion energy losses are about 3 times larger than electron energy losses for $\delta_w=0$, both become similar for $\delta_w\sim 60\%-70\%$, and electron energy losses become two orders of magnitude larger than ion ones in the CSR. If there is an ion axial flow of (average) velocity v_{xi}, the total losses of ion energy include the axial contribution $g_{riQ}\frac{1}{2}m_i v_{xi}^2$. In the acceleration region of a conventional Hall thruster and for charge-saturated conditions, this increment can be up to one order of magnitude. Figures 6(b)–6(c) show the evolution of electron and ion energy losses with T_1 and T_e. Notice the large gradients of q_{rpW} with T_e below the CSL. Again, the influence of the wall material disappears at the CSR, when q_{rpW} scales as $T_e^{3/2}$.

Since the net electrical current is zero and the sheaths are collisionless, the energy gained by the ions and the secondary electrons when crossing the sheath, $g_{riQ}e\phi_{WQ}$ and $|g_{rsQ}|e\phi_{WQ}$, respectively, is the energy lost by population p in the sheath QW, $g_{rpQ}e\phi_{WQ}$. Thus, the plasma energy flux into the wall W is equal to the energy flux across the presheath/sheath transition Q. The continuity of the energy flux across surface Q relates the energy flux deposited by population p into the wall to the energy lost by population e in the bulk of the plasma,

$$\begin{aligned} q_{reQ}&=q_{rpQ}-|q_{rsQ}|\\ &=\{q_{rpW}+e\phi_{WQ}(g_{rpQ}-|g_{rsQ}|)\}\\ &=g_{riQ}\left(\frac{2T_p}{1-\delta_w}+e\phi_{WQ}\right). \end{aligned} \tag{34}$$

Since there are no volumetric sources of energy, this radial loss must be compensated by a positive energy contribution in the axial direction, which, in general, means an axial gradient of T_e.[12,15]

V. CONCLUSIONS

This presheath/sheath model with total thermalization of secondary emission is based on considering wall-emitted electrons as a free population within the thin, collisionless sheaths, and as part of a unique population of confined electrons within the presheath. As a consequence the populations of confined electrons to be considered in sheath and presheath are not identical. The presheath and the sheaths are solved separately and then matched using continuity equations for the plasmas density and fluxes. For the presheath, a two-species plasma model can be used, whereas the sheath model is an extension of the Hobbs–Wesson model to warm ions. There are differences on the expression of the ion sound speed in sheath and presheath; in particular there is a contribution of the SEE beam in the sheath side. The sonic condition for the ion flow at both the presheath and sheath sides has been postulated from well-established behaviors for related cases. This condition closes the presheath/sheath matching and relates the temperature of the confined electron populations in sheath and presheath. It is found that, even at charge saturation, the density of secondary electrons entering the presheath is small and the temperatures of the confined electron populations in sheaths and presheath are similar.

The complete sheath/presheath solution for a plasma flowing axially between two annular walls depends on five

dimensionless parameters: β, $\tilde{v}_i$, $\tilde{v}_r$, $\tilde{T}_{iM}$, and T_1/T_e. The first four parameters determine the presheath solution, whereas the sheath solution depends on the two last ones. The similarity between the charge-saturation condition of Hobbs and Wesson and the Langmuir condition for a strong double layer has been stood out. A nonzero ion temperature does not modify the SEE yield necessary for charge-saturation, but diminishes the relative sheath potential drop at the charge-saturation regime. Taking into account the dependence of δ_w on the wall material, the sheath potential drop presents a maximum for an intermediate value of δ_w and a relative minimum at the charge-saturation limit; then, it becomes proportional to the electron temperature and universal for any wall material.

The potential drops in the inner and outer presheaths are never negligible. Furthermore, they can be larger than the sheath drops for large secondary emissions and large radial frictions. For annular channels, the inner and outer presheaths are asymmetric, but the two sheaths are practically identical (for the same wall material). An important conclusion is that the plasma current lost into the walls is determined totally by the presheath solution (that is, channel geometry and conditions of the bulk of the plasma). The wall material determines the sheath solution and the energy lost into the wall per particle. Electron energy losses change drastically with the SEE yield. On the contrary, ion energy losses depend weakly on δ_w, have a contribution from the plasma axial flow, and dominate for low secondary emission.

The model developed here is for total thermalization of the SEE, which corresponds to the collisional regime, $\lambda_d \ll \lambda_{\mathrm{col}} \ll h_c$. For the collisionless and weakly-collisional regimes, (i.e., $\lambda_{\mathrm{col}} \gg h_c$), most secondary electrons will cross the whole presheath from their emission wall and will be collected at the opposite wall if there is no potential barrier preventing it. For instance, for the potential profile of Fig. 5(a), $\lambda_{\mathrm{col}}/h_c \to 0$, and cold walls, electrons emitted from the outer wall will be collected back at the inner wall, whereas electrons emitted from the inner wall will be reflected back at the outer wall and then collected by the inner wall too. However, the presence of "free" populations of secondary electrons modifies the profile of the electric potential in sheaths and presheath. The amount of "free" SEE and the self-consistent potential profile are two coupled issues, which require more general models of sheath and presheath, than the ones developed here.

ACKNOWLEDGMENTS

The author thanks the aid from F. I. Parra for his contribution to this work and M. Martínez-Sánchez for helpful discussions.

This work was supported by the European Office for Aerospace Research and Development, under Contract No. F61775-01-WE070 (supervised by Dr. Ingrid Wysong).

[1] L. Tonks and I. Langmuir, Phys. Rev. **34**, 876 (1929).
[2] E. Harrison and W. Thompson, Proc. Phys. Soc. London **74**, 145 (1959).
[3] G. Emmert, R. Wieland, A. Mense, and J. Davidson, Phys. Fluids **23**, 803 (1980).
[4] R. Bissell, P. Johnson, and P. Stangeby, Phys. Fluids B **1**, 1133 (1989).
[5] J. Scheuer and G. Emmert, Phys. Fluids B **2**, 445 (1990).
[6] E. Ahedo, Phys. Plasmas **9**, 3178 (2002).
[7] L. Jolivet and J.-F. Roussel, in *SP-465: 3rd Spacecraft Propulsion Conference, Cannes* (Francia) (European Space Agency, Noordwijk, The Netherlands, 2000), pp. 367–376.
[8] C. Ordonez and R. Peterkin, J. Appl. Phys. **79**, 2270 (1996).
[9] G. Hobbs and J. Wesson, Plasma Phys. **9**, 85 (1967).
[10] L. Schwager, Phys. Fluids B **5**, 631 (1993).
[11] K. Stephens and C. Ordonez, J. Appl. Phys. **85**, 2522 (1999).
[12] E. Ahedo, P. Martínez-Cerezo, and M. Martínez-Sánchez, in *37th Joint Propulsion Conference, Salt Lake City, UT* (American Institute of Aeronautics and Astronautics, Washington, D.C., 2001), AIAA 2001–3323.
[13] Y. Raitses, J. Ashkenazy, and G. Appelbaum, in *25th International Electric Propulsion Conference, Cleveland, Ohio* (Electric Rocket Propulsion Society, Cleveland, OH, 1997), IEPC 97-056.
[14] J. Fife, M. Martínez-Sánchez, and J. Szabo, in *33rd Joint Propulsion Conference, Seattle, WA* (American Institute of Aeronautics and Astronautics, Washington, D.C., 1997), AIAA 97-3052.
[15] E. Ahedo, P. Martínez-Cerezo, J. Gallardo, and M. Martínez-Sánchez, in *27th International Electric Propulsion Conference, Pasadena, CA* (Electric Rocket Propulsion Society, Cleveland, OH, 2001), IEPC 01-17.
[16] V. Kim, J. Propul. Power **14**, 736 (1998).
[17] I. Langmuir, Phys. Rev. **33**, 954 (1929).
[18] M. A. Raadu, Phys. Rep. **178**, 26 (1989).
[19] S. H. Lam, Phys. Fluids **8**, 73 (1965).
[20] M. Keidar, I. Boyd, and I. Beilis, Phys. Plasmas **8**, 5315 (2001).